Proton conductivity in quasi-one-dimensional hydrogen-bonded systems: Nonlinear approach

George P. Tsironis
Institute for Nonlinear Science and Department of Chemistry (B-040), University of California, San Diego, La Jolla, California 92093

Stephanos Pnevmatikos
Center for Nonlinear Studies, Los Alamos National Laboratory, Los Alamos, New Mexico 87545 and Research Center of Crete, P.O. Box 1527, 71 110 Heraklio, Crete, Greece

(Received 1 August 1988)

Defect formation and transport in a hydrogen-bonded system is studied via a two-sublattice soliton-bearing one-dimensional model. Ionic and orientational defects are associated with distinct nonlinear topological excitations in this model. The dynamics of these excitations are studied both analytically and with the use of numerical simulations. It is shown that the two types of defects are soliton solutions of a double-sine-Gordon equation which describes the motion of the protons in the long-wavelength limit. With each defect there is an associated deformation in the ionic lattice that, for small speeds, follows the defect dynamically albeit resisting its motion. Free propagation as well as collision properties of the proton solitons are presented.

I. INTRODUCTION

Electrical conductivity in hydrogen-bonded crystals is an old problem that recently has been revived with the introduction of new techniques and ideas from nonlinear physics. As with several other problems in biology, such as (for instance) the dynamics of biopolymers, it provides a new and exciting arena where nonlinear, soliton-type modes might be responsible for energy and charge transfer.[1-3] Hydrogen bonding is not only ubiquitous in living matter but it also provides the dominant mechanism for crystallization in a variety of chemical substances, such as hydrogen halides.[4] An understanding of the electrical properties of systems with hydrogen bonds will provide information for a wealth of physical and biological systems and processes ranging from "simple" systems such as ice to the more complicated processes of proton transport across cellular membranes, the proton pump, or the dynamics of protons in the vision-related molecule rhodopsin.[5]

A great deal of activity has been devoted to the understanding of the physical and electrochemical processes that are responsible for the anomalously high proton mobility in the most common hydrogen-bonded crystal, ice. Onsager associated the conductivity in ice, which is not electronic but protonic in nature, to a hopping mechanism that allows the protons of the hydrogen bonds to move along hydrogen-bonded atomic channels.[6] Experimental evidence strongly indicates that charge transport proceeds via the motion of two types of defects that can be present in the network, viz., the ionic defects and the orientational (or Bjerrum) defects.[7-11] The former involve an intrabond motion of the (unique) binding proton, whereas the latter result from interbond or interatomic motion of the protons due to rotations of the water molecules. Weiner and Askar[12] introduced the idea of a collective transition of the interacting proton system that could explain qualitatively the ionic-defect creation and motion and suggested that an analogy holds with the creation and movement of dislocations in crystals.

More recently, Antonchenko, Davydov, and Zolotariuk (ADZ) (Ref. 13) focused their attention on explaining quantitatively the creation and transfer of ionic defects in hydrogen-bonded systems. They introduced a two-sublattice model (ADZ model) in which proton transport in an infinite one-dimensional chain (realized physically in ice through a Bernal-Fowler filament[14]) can proceed collectively via the propagation of two-component ϕ^4 solitons at a given characteristic velocity v_0. Lyapunov stability[15] and stability of solitons during collisions[16] have been studied, and a variety of interesting dynamical properties have been detected[17] for the ADZ model. Some extensions to other hydrogen-bonded configurations were introduced,[18,19] including a thermal activation mechanism for the ionic defects.[20] Finally, the interesting case of a quadratic phonon coupling was shown to lead to exact soliton solutions with rich dynamical properties.[21]

With regard to the orientational defects, there have been recent attempts aiming at the understanding of their formation and dynamics. The original Bjerrum picture[7] has been replaced by a collective-mechanism representation either by a direct incorporation of the dipole-dipole interaction in the Hamiltonian,[22,23] or via other effective approaches.[24]

Although the aforementioned models provide quantitative information regarding the collective proton dynamics that stems from the nonlinear structure of the hydrogen bond, they all suffer from the same defect, viz., they take into account only one or the other of the possible

two types of defects in the hydrogen-bonded networks. This is very restrictive, especially since there exists an abundance of experimental evidence[8–11] that clearly suggest that *both* types of defects participate in the transfer of charge across the hydrogen-bonded network.

The incorporation of both ionic and Bjerrum defects into a single classical model has been introduced recently.[25] In this model the essential physical requirements of the hydrogen-bonded networks were introduced and the resulting solvable collective dynamics was shown to lead to defect creation and propagation in the form of two-component solitons. In the present paper we extend the model introduced in Ref. 25 and begin a thorough analytical as well as numerical study of its static and dynamical properties. We emphasize that our present study addresses for the first time quantitatively, both analytically and by the use of numerical experiments, the simultaneous collective dynamics of *both* types of defects present in ice and other hydrogen-bonded materials.

In the present paper we will restrict ourselves to the exposition and analytical study of the two-defect model and emphasize its physical consequences. We will present numerical simulations for the model that support and extend the analytically derived results. In particular, we will present numerical experiments that determine the free propagation and collision properties of the defects. Some aspects of defect dynamics in the presence of an externally applied electric field have been presented elsewhere.[26]

The structure of the present paper is as follows: In Sec. II we describe the two-defect model in detail. We give the classical Hamiltonian for the system (Sec. II A) and discuss the physics of the assumed substrate potential as well as the interaction potential. In Sec. II B we discuss the degeneracy of the ground states, in Sec. II C we derive the dispersion relations in the harmonic approximation, and in Sec. II D we write the equations of motion in the continuum limit and give their solutions. In Sec. III we describe the numerical simulations performed and analyze the free propagation of the solitons and in particular study their collision properties. Finally, in Sec. IV we conclude by discussing the physics of the collisions as well as other properties of the discrete system.

II. DESCRIPTION OF THE MODEL AND ANALYTICAL RESULTS

A typical one-dimensional hydrogen-bonded network consists of two coupled sublattices: One is that of the negative ions (or a group of atoms), and the other is that of protons. In a one-dimensional geometry, this configuration would be represented by

$$\cdots X\text{—H}\cdots X\text{—H}\cdots X\text{—H}\cdots X\text{—H}\cdots , \qquad (2.1)$$

where X denotes an ion (usually O, F, or N) or an aggregate, and H is a hydrogen that is bonded covalently with an adjacent ion (full link) and forms a hydrogen bond with another ion (dotted link). The covalent and hydrogen bonds in a X—H $\cdots$ X configuration are interchangable, viz., the proton in the bond that links the two X ions together can tunnel between two equilibrium positions that are energetically equivalent. Thus, the nature of the effective potential for the proton is that with two stable equilibrium positions separated by an unstable one. A typical example of such a potential for the proton in the hydrogen bond[20] is the well-known double-well potential, viz.,

$$V(x)=-\tfrac{1}{2}ax^2+\tfrac{1}{4}bx^4 ,$$

where a, b depend on the specific system under study.

Because of the double-well structure of the interion bond, there are two equilibrium configurations for the extended system; one with all the protons in one minimum (say left) and the other when all protons are in the other minimum (say right). Excitations from either of these equilibrium configurations, i.e., spatially localized transitions from one ground-state configuration to the other result to (domain-wall-type) defects in the lattice. These defects carry effective charge (positive or negative) and are called *ionic defects*. In the case of ice, i.e., when the X ions are oxygens, there are two types of ionic defects, viz., hydroxyl ion (OH^-) with negative effective charge and hydronium ion (H_3O^+) with positive effective charge. The spontaneous creation and propagation of these defects has been studied extensively and their dynamics have been used to explain some of the electrical properties of the ice crystals.[8–11]

In the past, models with double-well potentials for the interion linkage have been studied systematically in the context of the dynamics of protons in hydrogen-bonded systems. Such models have been shown to lead to kink solitons that represent the ionic defects in the crystal.[12,13,15–21,27] The main disadvantage of such potentials, however, is that they cannot take into account the orientational defects that are known to be present in a hydrogen-bonded system. The latter defects are due to rotations of entire water molecules (in ice) with a net result being the appearance of a second proton in a given hydrogen bond (D-Bjerrum defect) or the disappearance of a proton from a bond resulting in an empty bond (L-Bjerrum defect). Since macroscopic charge transfer in hydrogen-bonded systems involves both kinds of defects, all models that are based on such a type of potential can provide only partial information on the dynamics of protons. In particular, conduction properties of the protons cannot be addressed with such potentials.

To circumvent these difficulties, it is necessary to adopt model substrate potentials for the protons that, on one had, retain the topology of the double-well potential which is essential for the proper description of the hydrogen bond, and, on the other hand, allow for an effective charge transfer between adjacent hydrogen bonds that comes as a result of the Bjerrum rotations. This can be accomplished with the introduction of a doubly periodic substrate that can accommodate both types of defect formation that are known experimentally to play important roles in the electrical properties. We proceed by describing the double-defect model.

A. The Hamiltonian

The total Hamiltonian H of a quasi-one-dimensional system, described through the present model, consists of three parts, i.e.,

$$H=H_p+H_o+H_i \ , \tag{2.2}$$

where H_p is the Hamiltonian for the proton sublattice, H_o for the ion sublattice, and H_i is the interaction term between the two. We have

$$H_p=\sum_n \left[1/2m \left[\frac{dy_n}{dt} \right]^2 + 1/2K_1(y_{n+1}-y_n)^2 + S_p V_1 \left[\frac{4\pi}{l_0} y_n \right] \right] , \tag{2.2a}$$

$$H_o=\sum_n \left[1/2M \left[\frac{dY_n}{dt} \right]^2 + 1/2K_2(Y_{n+1}-Y_n)^2 + S_0 V_2 \left[\frac{Y_n}{l_0} \right] \right] , \tag{2.2b}$$

$$H_i=\chi \sum_n \left[(Y_n-Y_{n-1}) \Phi \left[\frac{4\pi}{l_0} y_n \right] \right] . \tag{2.2c}$$

In Eqs. (2.2), m, M denote the mass of the protons and ions, respectively, K_1, K_2 the corresponding spring constants, and χ is the coupling parameter between the two interacting sublattices. The displacement y_n of the nth proton is measured from the central unstable equilibrium position in the hydrogen bond, i.e., from the middle of the bond that links the ions, whereas Y_n, the displacement of the nth ion, is measured from its equilibrium position. The equilibrium distance between two heavy ions is taken to be l_0. We assume that in both chains, only the nearest neighbors interact among themselves. The combined effects of Coulomb repulsion and screening are included in the on-site potentials, for both sublattices.[28] It is appropriate to introduce the following dimensionless quantities:

$$u_n=\frac{4\pi}{l_0} y_n, \quad w_n=\frac{Y_n}{l_0} \ . \tag{2.3}$$

With these definitions, the substrate potentials in Eqs. (2.2) are written

$$V_1(u_n)=\frac{2}{1-a^2}\left[\cos\left[\frac{u_n}{2} \right]-a \right]^2, \quad 0<a<1 \ , \tag{2.4a}$$

$$V_2(w_n)=\tfrac{1}{2}w_n^2 \ , \tag{2.4b}$$

while for the interaction term of Eq. (2.2c), the function $\Phi(u_n)$ is defined

$$\Phi(u_n)=\cos\left[\frac{u_n}{2} \right]-\cos\left[\frac{u_0}{2} \right], \quad u_0=2\arccos(a) \ . \tag{2.4c}$$

The potential $V_1(u_n)$ is the on-site potential for the proton sublattice (Fig. 1) and it is chosen to satisfy the physical requirements posed by a hydrogen-bonded network. If we assume that the rest ion position is where the larger maximum occurs, then the two local minima separated by the smaller maximum represent the two-proton equilibrium positions within the hydrogen bond, and the larger barrier represents the energy necessary for a Bjerrum rotation to take place. If a proton has enough energy, such rotation is possible, and the proton can move to the other side of the large barrier. The activation energy for such a rotation in ice is larger than the one for the creation of an ionic defect. This is so because the former results only after two bonds are broken. In systems where this might not be true,[4] a different value in the parameter a is necessary.

One disadvantage of the potential of Eq. (2.4c) is that it depends only on one parameter, viz., a. Consequently, one cannot assign independent values to the relative maxima of the potential. With the proper choice of the parameter a, however, we can simulate the respective values of the hydrogen-bond barrier and the Bjerrum rotation energy to reasonable accuracy for several hydrogen-bonded systems.

$V_2(w_n)$ is an on-site harmonic potential that acts on the heavy ions. This potential is created from the interaction of the quasi-one-dimensional chain under study with the rest of the crystal and guarantees the rigidity of the lattice. The parameter S_0 in Eq. (2.2b) measures the strength of this effective interchain interaction. Finally, the potential function $\Phi(u_n)$ determines the interaction between the two sublattices. The functional form of this term is restricted by the requirement that when either sublattice is at an equilibrium position, the interaction term of the Hamiltonian in Eq. (2.2c) must be zero. The particular form chosen in Eq.(2.4c) clearly has these properties, and its choice has been dictated by the specific form of the substrate potential $V_1(u_n)$. As we will shown shortly, for this coupling, analytical solutions to the equations of motion can be found.

In Fig. 2(a), we compare the potential $\Phi(u)$ with the

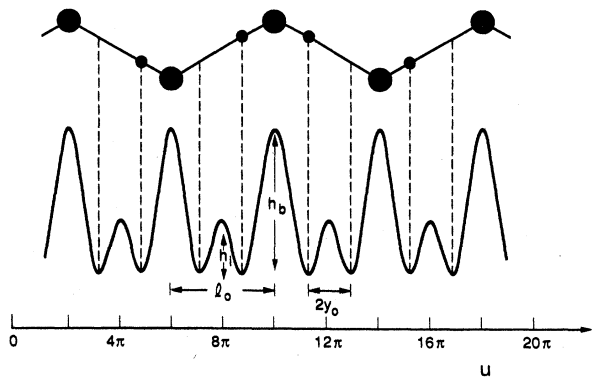

FIG. 1. The substrate potential $V_1(u)$ is plotted as a function of the distance along a hydrogen-bonded network. The heavy ions (large solid circles) and the protons (small solid circles) are shown in the zig-zag geometry of a hydrogen-bonded network. The periodicity of the on-site potential $V_1(u)$ is 4π and a is equal to 0.6486.

on-site potential $V_1(u)$. We observe that $\Phi(u)$ has its maximum value at the top of the hydrogen-bond barrier and its minimum in the location of the ions. This dependence leads to the following behavior in the interaction term of Eq. (2.2c): Let us assume that the difference in the displacements of the ions, $Y_n - Y_{n-1}$, is positive, leading to a local rarefaction in the ion sublattice, and that the coupling parameter χ is positive as well. In this case then, the form of the interaction potential $\Phi(u)$ favors a tendency of the protons to move away from the ionic barrier and closer to the ions in either side of the hydrogen bond, due to the even symmetry of the potential. As a result, we have an effective reduction of the rotational barrier (large barrier). On the other hand, when there is a compression in the ionic sublattice, then $Y_n - Y_{n-1} < 0$, and we now have a reduction in the ionic barrier. This situation is depicted in Fig. 2(b) where there is a comparison of the substrate potential with $-\Phi(u)$. We conclude, that when χ is positive, a compression wave in the ions will help in the creation and the motion of the ionic defects, whereas a rarefaction wave will tend to help the motion of the Bjerrum defects. Clearly, the opposite holds, for negative χ. The sign of the nonlinearity parameter plays an important role in the physics of the problem and it will have to be determined according to the specific system under study.

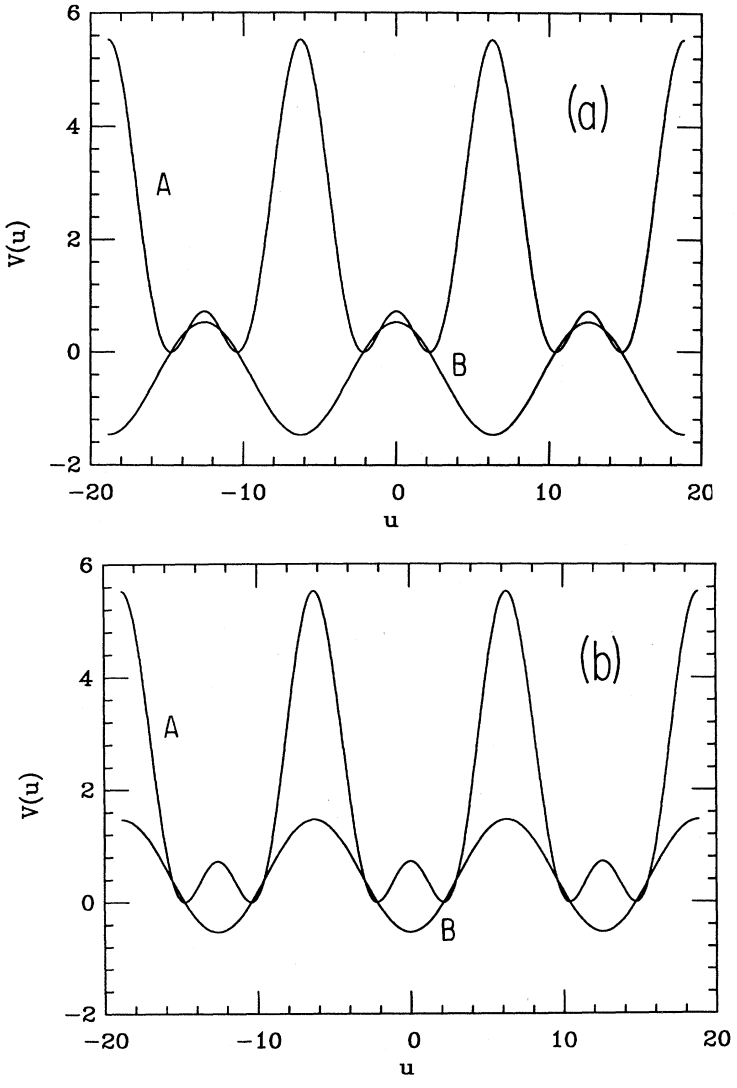

FIG. 2. The substrate potential V_1 (curve A) is compared with (a) the interaction function $\Phi(u)$ (curve B) as a function of distance, and (b) with $-\Phi(u)$ (curve B). The former case favors Bjerrum defect motion whereas the latter reduces the hydrogen-bond barrier and thus favors ionic defect motion.

The equations of motion for the Hamiltonian of Eq. (2.2) can be written, in dimensionless form, as follows:

$$\frac{d^2u_n}{d\tau^2}=\omega_1^2(u_{n+1}-2u_n+u_{n-1}) -\Omega_1^2\frac{dV_1(u_n)}{du_n}-\chi_1(w_n-w_{n-1})\frac{d\Phi(u_n)}{du_n} , \quad (2.5a)$$

$$\frac{d^2w_n}{d\tau^2}=\omega_2^2(w_{n+1}-2w_n+w_{n-1}) -\Omega_2^2\frac{dV_2(w_n)}{dw_n}+\chi_2[\Phi(u_{n+1})-\Phi(u_n)] . \quad (2.5b)$$

In Eqs. (2.5) as well as in what follows, we use the following units:

energy: $\varepsilon_0=(1.986\times10^{-23})J$,

time: $t_0=\omega_2^{-1}=(M/K_2)^{1/2}$,

length: l_0 .

With these choices, energy is measured in cm^{-1} and for mass and force we have the following derived units:

mass: $m_0=\varepsilon_0 t_0^2/l_0^2$,

force: $f_0=\varepsilon_0/l_0$,

potential constant: $K_0=\varepsilon_0/l_0^2$.

This system of units is introduced in order to facilitate the numerical computations and to enable the comparison of the results with experiments. Using the preceding defined fundamental and derived units, we determine the values of the constants and parameters that are present in the equations of motion in Eqs. (2.5):

$$\omega_1=\left[\frac{K_1m_0}{K_0m}\right]^{1/2}=t_0\left[\frac{K_1}{m}\right]^{1/2} ,$$

$$\omega_2=\left[\frac{K_2m_0}{K_0M}\right]^{1/2}=t_0\left[\frac{K_2}{M}\right]^{1/2}=1 ,$$

$$\chi_1=(4\pi)^2\frac{\chi m_0}{f_0m}=\frac{(4\pi)^2t_0^2\chi}{ml_0} ,$$

$$\chi_2=\frac{\chi m_0}{f_0M}=\frac{t_0^2\chi}{Ml_0} ,$$

$$\Omega_1=\frac{4\pi}{l_0}\left[\frac{S_p}{m}\right]^{1/2}t_0 ,$$

$$\Omega_2=\frac{1}{l_0}\left[\frac{S_0}{M}\right]^{1/2} t_0 .$$

With these definitions, all coefficients are dimensionless.

For the specific case of the ice crystal that we are considering in the simulations (in Sec. III), we have chosen values for the parameters that are consistent with the recent literature on the subject. We take $t_0=2.0\times10^{-13}$, $l_0=2.7\times10^{-10}$, $m=1.67\times10^{-27}$, and $M=2.84\times10^{-26}$. The actual value for the coupling coefficient χ is not known with accuracy since there are several uncertainties regarding even the exact form of the interaction term. For a coupling coefficient $\chi=1.0\times10^{-10}$, χ_1 and χ_2 become 1.4×10^3 and 0.52, respectively. In the simulations we are reporting in the present paper, we chose a substantially smaller value for χ; larger values in the coupling enhance the stability of the nontopological excitation in the ionic sublattice.[29]

B. Ground states

In its ground state, the system can be found in two energetically equivalent, but topologically distinct, configurations. Both of these states occur when the heavy ions are in equilibrium, i.e., when $w_n=0$ and all protons occupy equivalent minima of the periodic substrate potential, i.e., $u_n=4\pi n\pm u_0$.

The period of the on-site potential for the protons is 4π. Within one period, the potential $V_1(u)$ has a local maximum for $u=0$, and a global maximum at $u=2\pi$. The corresponding heights of the barriers are

$$V(0)=2\frac{1-a}{1+a} \text{ and } V(2\pi)=2\frac{1+a}{1-a} ,$$

times the coefficient S_p. We note, that once a is chosen, the relative strengths of the potential barriers are fixed. The parameter a determines the relative distance between the maxima and minima in the potential as well, since the first minimum occurs at the value $u_{\min}=u_0=2\arccos(a)$.

C. Harmonic limit

When the amplitude of the motion of the particles in the system is small, we can approximate Eqs. (2.5) with a new set of coupled equations. For this linearization procedure to take place, we assume that the displacement y_n of the nth proton from its equilibrium position $\pm u_0$ is small, and the corresponding small displacement of the nth ion is w_n. We now have the following equations of motion:

$$\frac{d^2y_n}{d\tau^2}=\omega_1^2(y_{n+1}-2y_n+y_{n-1})-\Omega_1^2y_n\mp\chi_1'(w_n-w_{n-1}) , \tag{2.6a}$$

$$\frac{d^2w_n}{d\tau^2}=\omega_2^2(w_{n+1}-2w_n+w_{n-1})-\Omega_2^2w_n\pm\chi_2'(y_{n+1}-y_n) , \tag{2.6b}$$

where

$$\chi_1'=\frac{\chi_1}{2}(1-a^2)^{1/2},\quad \chi_2'=\frac{\chi_2}{2}(1-a^2)^{1/2} ,$$

and the upper (lower) sign refers to equilibrium position $+u_0$ $(-u_0)$, with $u_n=\pm u_0+y_n$.

The equations of motion (2.6) represent two coupled linear chains of vibrating masses. Each mass in either chain vibrates around an equilibrium position under the influence of a harmonic potential and is coupled to the nearest-neighboring masses with linear springs. The two chains couple through the last terms (on the right-hand side) in Eqs. (2.6a) and the interaction energy between the two is bilinear in the displacements.

In order to calculate the low-amplitude vibration dispersion relations, we assume solutions of the form

$$y_n=ye^{-\omega\tau}e^{ikn},\quad w_n=we^{-i\omega\tau}e^{ikn} . \tag{2.7}$$

Upon substitution of Eqs. (2.7) in Eqs. (2.6), we obtain

$$(-\omega^2+\rho_1^2)y\pm\chi_1'(1-e^{ik})w=0 , \tag{2.8a}$$

$$\pm\chi_2'(1-e^{-ik})y+(-\omega^2+\rho_2^2)w=0 , \tag{2.8b}$$

$$\rho_1^2=\Omega_1^2+4\omega_1^2\sin^2\frac{k}{2},\quad \rho_2^2=\Omega_2^2+4\omega_2^2\sin^2\frac{k}{2} . \tag{2.8c}$$

When the coupling between the two chains is zero, the dispersion relation consists of two branches given by ρ_1 and ρ_2. This is depicted in Fig. 3(a), where the upper branch is the proton dispersion curve and the lower one is the ion dispersion curve. These dispersion curves are modified when we turn the coupling on. The new dispersion relation can be easily evaluated from the diagonalization of the coefficient matrix in Eqs. (2.8) leading to

$$\omega^2(k)=\frac{\rho_1^2+\rho_2^2}{2}\pm\left[\left[\frac{\rho_1^2-\rho_2^2}{2}\right]^2+\chi_1'\chi_2'\sin^2\frac{k}{2}\right]^{1/2} . \tag{2.9}$$

As χ increases, the lower branch becomes flatter at $k=0$, whereas the upper branch becomes steeper in the same point. This has the effect of increasing the sound velocity in the proton sublattice and decreasing the sound velocity in the ionic sublattice. Therefore, as χ increases, large-wavelength waves move relatively slower in the ion lattice but relatively faster in the proton lattice. This situation is depicted in Figs. 3(b) and 3(c) for some larger χ values.

D. Continuum limit

Although the physical hydrogen-bonded network is a system with discrete symmetry, analytical results can only be obtained in the continuum limit, where the excitations are assumed to extend over large distances compared to the lattice spacing. In this limit, Eqs. (2.6) become

$$u_{\tau\tau}-c_0^2u_{xx}+\Omega_1^2\frac{dV_1}{du}+\chi_1w_x\frac{d\Phi}{du}=0 , \tag{2.10a}$$

$$w_{\tau\tau}-v_0^2w_{xx}+\Omega_2^2\frac{dV_2}{dw}-\chi_2\frac{d\Phi}{dx}=0 , \tag{2.10b}$$

where x,τ are the dimensionless space and time variables, $c_o=\omega_1$, $v_o=1$ represent the speed of sound in the proton-

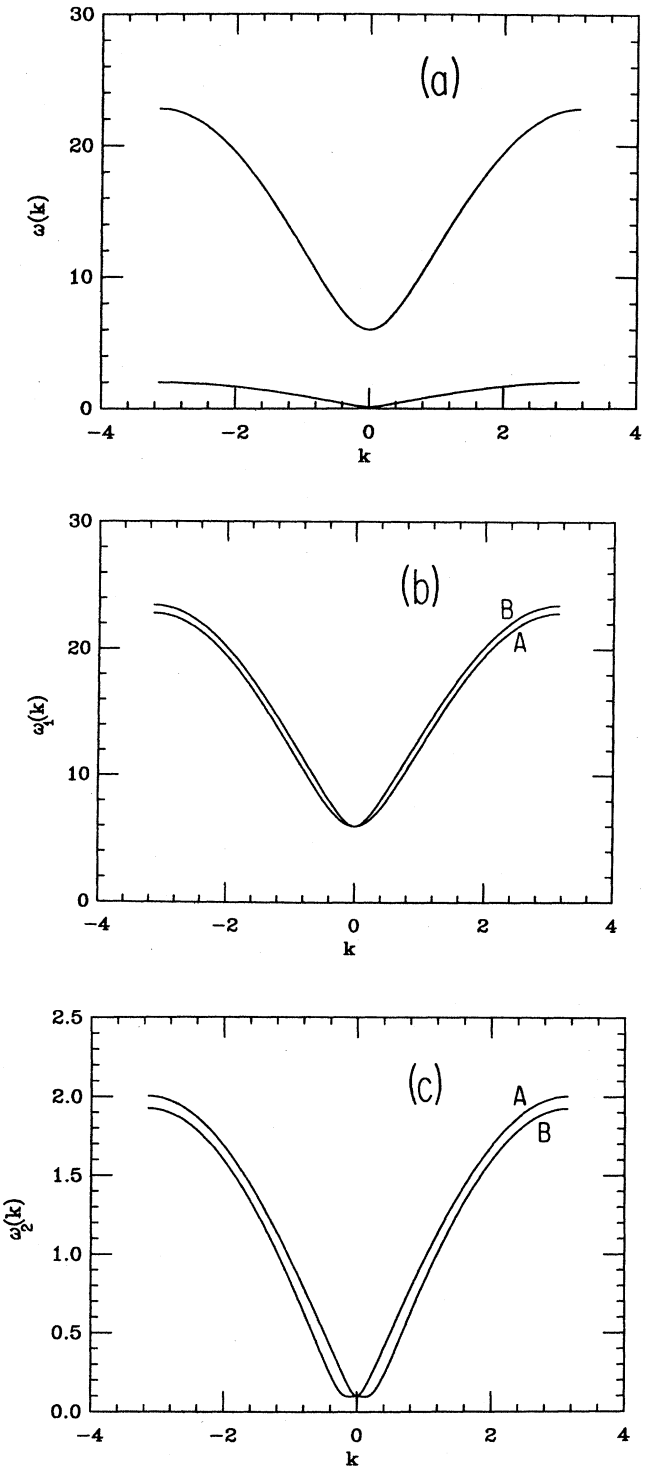

FIG. 3. In (a) the dispersion curve $\omega(k)$ vs k is plotted for both sublattices and for the value of the nonlinearity parameter that has been used in the simulations. In (b) $\omega_1(k)$, the dispersion curve for the harmonic proton motion is presented (curve A) and compared with the one obtained for larger χ (curve B; the value of the nonlinearity parameter is 100 times larger than the one used in the simulations). In (c) $\omega_2(k)$, the dispersion curve for ions is shown (curve A) and compared with tone for which χ is ten times larger (curve B).

ic and ionic sublattice, respectively, χ_1, χ_2 are proportional to χ, and Ω_1, Ω_2 are proportional to $S_p^{1/2}$, $S_0^{1/2}$, respectively.

In the special case when $\Omega_2=0$, Eqs. (2.10) lead to a double-sine-Gordon equation for the protonic sublattice

$$(v^2-c_0^2)u_{\xi\xi}+\varepsilon\left[-\sin u+2a\sin\left[\frac{u}{2}\right]\right]=0\ , \quad (2.11a)$$

while for the heavy sublattice we have

$$w_\xi=\frac{\chi_2}{v^2-v_0^2}\left[\cos\left[\frac{u}{2}\right]-a\right]\ , \quad (2.11b)$$

with

$$\varepsilon=\frac{\Omega_1^2}{1-a^2}\frac{\chi_1\chi_2}{4(v_0^2-v^2)}\ , \quad (2.11c)$$

where $\xi=x-v\tau$ and v is the travelling wave velocity. The parameter ε defines a new effective barrier height for the double-sine-Gordon equation; when $\chi=0$ the known results are recovered.[30-32] For $\chi_1,\chi_2\propto\chi\neq0$ this coefficient contains the influence of the heavy sublattice on the ionic one. We observe that for travelling velocities smaller than v_o, the effective barrier decreases, whereas the opposite effect occurs for $v>v_o$; this holds *independently* of the sign of the coupling coefficient χ. On the other hand, the sign of $w_\xi(=w_x)$ in Eq. (2.11b) depends on the velocity v. When the travelling velocity v is equal to the value of the sound waves in the ionic sublattice, viz. v_o, Eqs. (2.11) seem to have a singularity, and for larger velocity values w_ξ changes sign. In this latter case an initially rarefacting tendency in the ionic lattice becomes compressive and vice versa. The apparent singularity,[26] the physics of which is discussed herein, disappears when $\Omega_2\neq0$.

As is well known, the double-sine-Gordon Eq. (2.11a) results in two types of kink solutions that in the present model represent ionic and Bjerrum defects, respectively. Equation (2.11b), on the other hand, defines an excitation in the heavy-ion sublattice that is formed because of the topological excitations of Eq. (2.11a). The non-traveling-wave solutions of Eqs. (2.11) can be obtained easily[30-32] they are given by

$$u_{\rm I}(x,\tau)=4\pi n\pm4\arctan\{R\tanh[K_s(x-x_0)-\Omega_s\tau]\}\ , \quad (2.12a)$$

$$u_{\rm II}(x,\tau)=(2n+1)(2\pi)\pm4\arctan\{R^{-1}\tanh[K_s(x-x_0)-\Omega_s\tau]\}\ , \quad (2.12b)$$

where

$$R=[(1-a)/(1+a)]^{1/2},\ K_s=\gamma\lambda/2d,\ \Omega_s=K_sv\ ,$$
$$\gamma=[1-(v/c_0)]^{-1/2},\ d=c_0/\Omega_1,\ \alpha=\cos(u_0/2)\ , \quad (2.12c)$$
$$\lambda=\left[1+\frac{\chi_1\chi_2}{4\Omega_1^2}\frac{1-\alpha^2}{v^2-v_0^2}\right]^{1/2}\ ,$$

for the protonic part. The solution for the heavy-ion motion can be easily obtained from inserting Eqs. (2.12) into Eq. (2.11b). After integration, two kink-type solutions are obtained for $w(x,\tau)$, the displacement from the equilibrium positions of the heavy masses in the ionic sublattice.

The static solutions of Eqs. (2.12) above provide two types of kinks for the protonic sublattice (small and large kink, and the corresponding antikinks), and for each of those, a nonlinear kink-type excitation in the ionic sublattice. When a kink is present in the protonic sublattice a deformation is created in the ionic sublattice that can travel with it, as long as the velocity of the kinks do not exceed the speed of sound in the ionic chain. When the velocity of the former is larger than that, the ionic deformation lags behind. In Figs. 4 and 5 we present the dou-

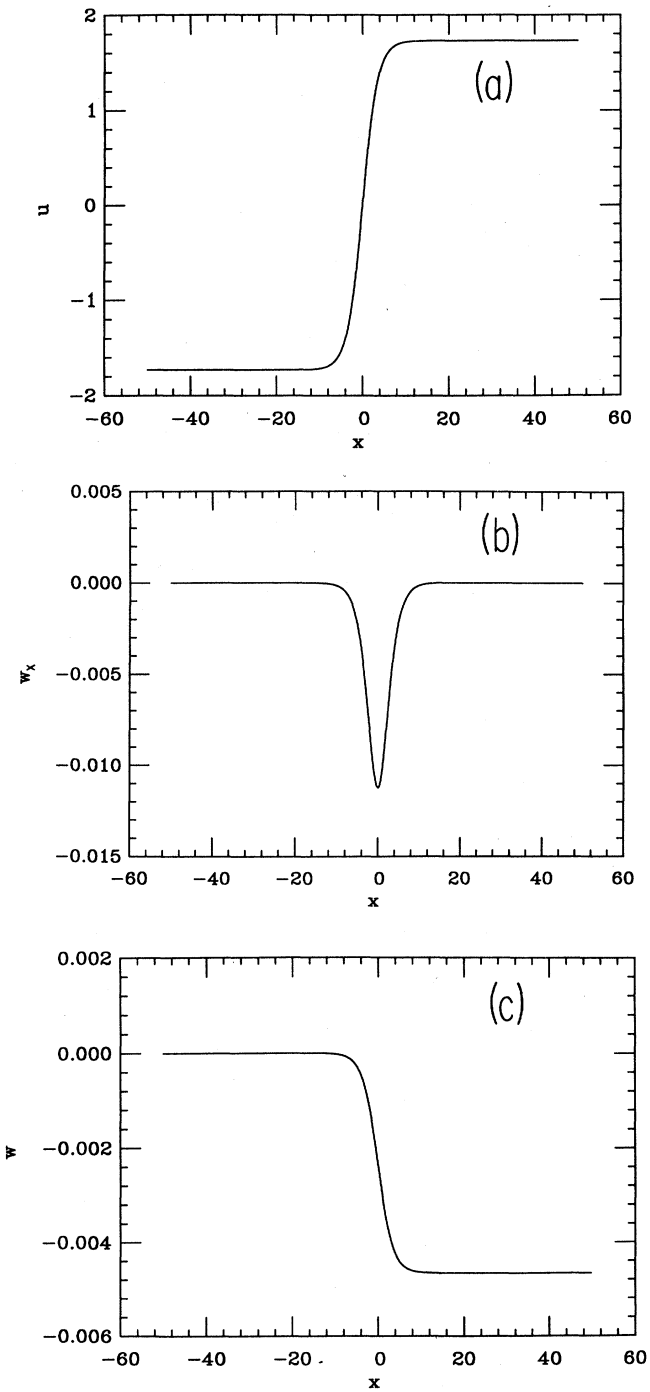

FIG. 4. Two-component solitons for $\Omega_2=0$. We plot in (a) the small kink (ionic defect), (b) the slope $w_x=dw/dx$ of the ionic deformation, and (c) the ionic deformation itself.

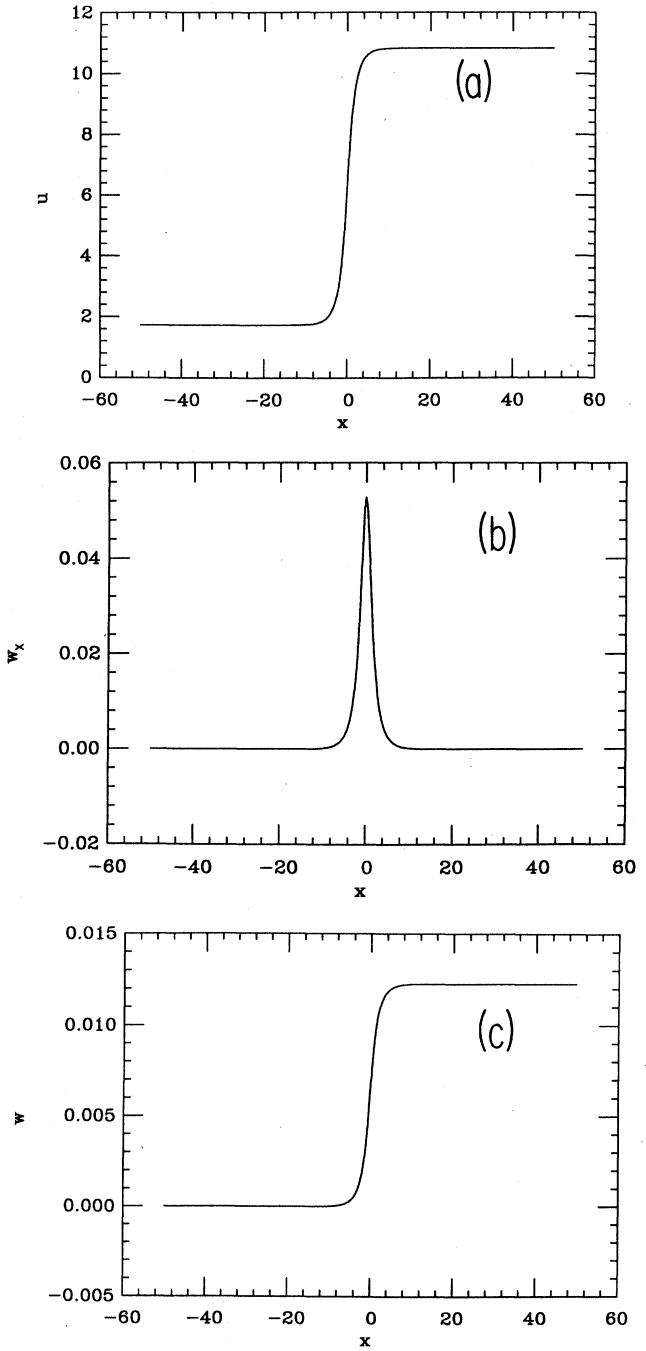

FIG. 5. Same as in Fig. 4, but for large kinks (Bjerrum defects). We show: In (a) a large kink, in (b) the slope of the induced ionic deformation, and in (c) its spatial dependence.

ble kink solutions for the two sublattices.

When $\Omega_2 \neq 0$, the shape of the deformation in the ionic lattice changes and analytical solutions of the form given by Eqs. (2.12) are no longer available. It is, however, possible to obtain an approximate solution for the composite nonlinear excitations for one particular value of the velocity of the moving excitation, i.e., when the latter moves with velocity $v = v_0$, which is the velocity of sound in the ionic lattice. For this velocity, Eq. (2.10b) becomes inertialess and we obtain

$$w = -\frac{\chi_2}{2\Omega_2^2} u_\xi \sin\frac{u}{2} \ . \tag{2.13}$$

The substitution of Eq. (2.13) into Eq. (2.10a) results in an equation which is more complicated than Eq. (2.11a), in that it contains a term proportional to u_ξ^2 as well as u-dependent coefficients. These additional terms, however, are proportional to χ_2 which is in the present case much less than 1 and therefore can be neglected to the lowest order. Consequently, Eqs. (2.12) are good approximate solutions for the present case of $\Omega_2 \neq 0$ and $v = v_0$ for the protonic sublattice (this is readily justified in the numerical simulations as well). Combining Eqs. (2.12) with (2.13), and after some straightforward algebra, we obtain the following forms for the nonlinear excitations in the ionic sublattices:

$$w_{\rm I}(x,\tau) = -\frac{2\chi_2}{\Omega_2^2} \frac{RK_s \operatorname{sech}^2[K_s(x-x_0)-\Omega_s\tau]}{1+R^2\tanh^2[K_s(x-x_0)-\Omega_s\tau]} \sin\frac{u_{\rm I}(x,\tau)}{2} \ , \tag{2.14a}$$

$$w_{\rm II}(x,\tau) = -\frac{2\chi_2}{\Omega_2^2} \frac{R^{-1}K_s \operatorname{sech}^2[K_s(x-x_0)-\Omega_s\tau]}{1+R^{-2}\tanh^2[K_s(x-x_0)-\Omega_s\tau]} \sin\frac{u_{\rm II}(x,\tau)}{2} \ , \tag{2.14b}$$

where $u_{\rm I}(x,\tau)$ and $u_{\rm II}(x,\tau)$ are given in Eqs. (2.12). In Fig. 6 we present the approximate solutions for the ionic sublattice with $\Omega = 0.1$. The proton soliton solutions correspond to those plotted in Figs. 4(a) and 5(a). It is evident that the shape of the ionic deformation caused by the protonic kink has changed dramatically from a kink-type to a gradient or shocklike wave. It is worth pointing out that the ionic deformation is asymmetric in terms of compression and rarefaction and it is quite different for the small and large kinks, respectively [this asymmetry was present in the ionic kinks as well as can be verified from Figs. 4(c) and 5(c)]. This is due to the different topological properties of the proton kinks and the choice of the interaction term (2.2c). It has been observed in the computer simulations of the system under study, that the ionic deformation depicted in Fig. 6 for the specific velocity v_0 survives approximately in almost all velocity regimes, although it does not retain the preceding given exact symmetric shape.

III. SIMULATIONS

In this section we present the results of the actual numerical experiments performed on the system. We have chosen a one-dimensional crystal with 400 ions and equal number of protons placed periodically with a lattice spacing l_0. The equations of motion for the discrete system were those given in Eq. (2.5). They were integranted numerically, using a fourth-order Runge-Kutta scheme with double precision arithmetics. The integration time step was kept the same for all simulations and equal to $\Delta t = 0.01$. With a typical time (in natural units) of $t_m = 100$, this amounts to $\Delta t \times t_m = 10\,000$ iterations, for a typical run. We choose fixed boundaries for the protonic chain and semifree for the ionic chain, viz., the first ion was kept fixed and the last ion was free to move. The initial conditions for the proton lattice were chosen according to the solutions of the double-sine-Gordon equation.

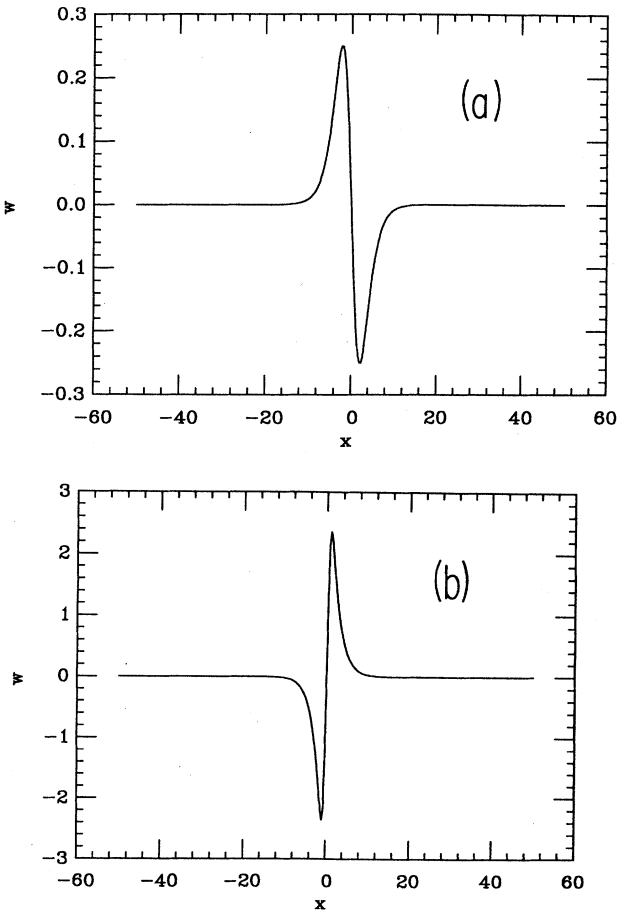

FIG. 6. In (a) we plot the ionic deformation induced by a small protonic kink on the ionic sublattice at the lower critical velocity v_0. We note the drastic change in the shape of the deformation as compared with that depicted in Fig. 4(c). In (b) we show the corresponding ionic deformation of a large kink.

The ionic lattice was taken to be initially at rest. As noted before, these are true solutions of the continuum equations of motion only when $\Omega_2=0$. In the simulations, we imposed a weak substrate potential ($\Omega_2=0.1$) and thus these are no longer exact solutions of the system. Since the actual value of the substrate is very small, this discrepancy does not affect appreciably the evolution of the proton solitons.

In the study of the dynamical properties of the nonlinear excitations of the system, two velocity values seem to be of particular importance; these are the velocity of sound in two sublattices, denoted with v_0 for the ionic and c_0 for the protonic one. For the present choice of parameter values and in dimensionless units these have the value 1.0 and 11.0, respectively. While $v \ll v_0$, i.e., for small kink velocities, both small and large excitations propagate freely carrying along the ionic lattice deformation. Upon increase of their velocity, however, and as it approaches the lower critical velocity v_0, the effective resistance that the ionic substrate exerts on them increases substantially. This effect is accompanied by a dramatic increase in the amplitude of the oscillations of the heavy ions, consistent with Eqs. (2.14), where $K_s \to \infty$ when $v \to v_0$. For initial kink velocities larger than v_0 the effective mobility of the kinks is much smaller than that for $v < v_0$. In fact, for relative small velocities compared to c_0, viz., $v \lesssim 5$, the propagation of the free solitons is quickly inhibited by the interaction with the ions. The sharp reduction of the mobility of the proton solitons at velocities comparable to v_0 is seen in the numerical simulations where mobilities are determined.

Having discussed briefly the properties of the free propagation of the proton kinks, we now come to their collision properties. We note here that our experimental conclusions regarding these properties seem to agree with the results of Campbell, Peyrard, and Sodano, who performed a thorough analysis of the properties of (one-component) kinks in the double-sine-Gordon equation.[32] That is, the presence of the ionic substrate, although profoundly altering the free kink dynamics, does not affect substantially their basic collision properties.

There are various pairs of solitons that can undergo a collision. Let us first consider a small kink-antikink pair; physically this corresponds to two different ionic defects with equal and opposite charge. In the numerical experiment, we place the kink-antikink pair in two distant positions in the one-dimensional system with several values of initial (opposite) velocities. We typically observe two effects in such a collision: (a) For relatively small initial velocities the solitons penetrate each other, annihilate, and in their place leave a spatially localized oscillation. This behavior corresponds to the trapping of the small kink-antikink double-sine-Gordon pair reported by Campbell *et al.* which is accompanied by a "decaying breather" type of final state. This decay is caused here by the coupling of the proton chain with the ionic one. The ionic chain acts effectively as a dissipative reservoir for the protons. (b) For larger velocities (typically for $v > 5.0$ an inelastic collision occurs and the two kinks do *not* pass through each other but *reflect*. This behavior persists till the upper critical velocity c_0 is reached. This property consistent with the findings of Campbell *et al.* as well; however, a conversion of two small kinks into two large ones as reported in Ref. 31 for the double-sine-Gordon equation, has not been observed in the system under study. Representative plots for the evolution of small kinks (ionic defects) are given in Figs. 7 and 8.

The evolution of the kink-antikink pair presented in Fig. 8 should be contrasted with the one in Fig. 7. In Fig. 7 the solitons are moving slower, whereas in Fig. 8 they

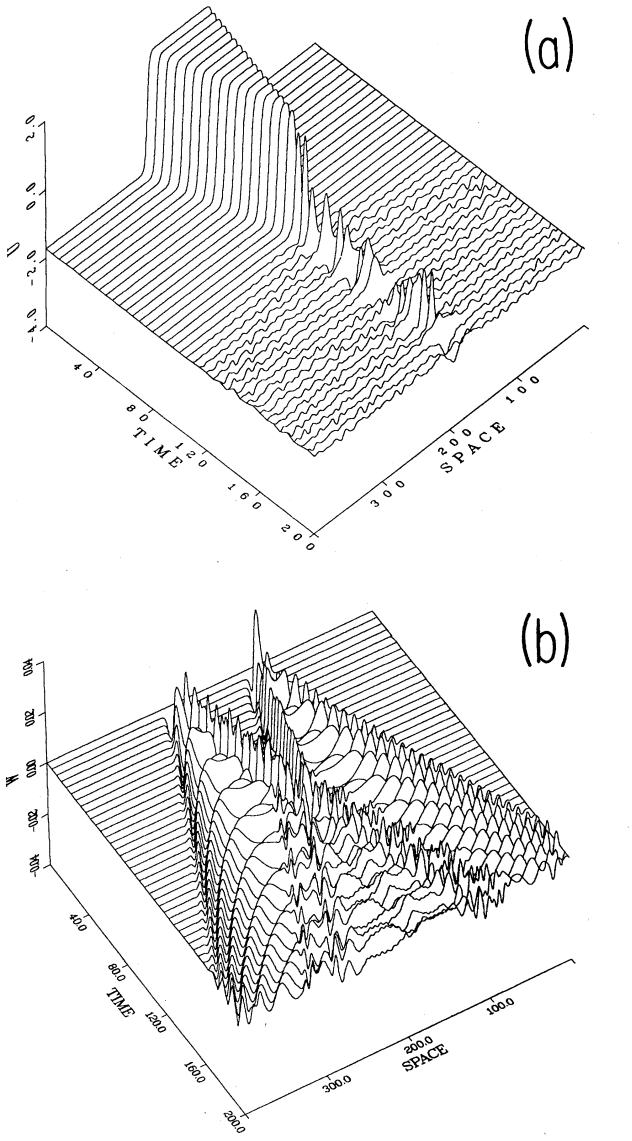

FIG. 7. Collision of two small kinks with small initial velocities. Initially we create a small kink with velocity $v=0.5$ in position 150 and a small antikink with velocity $v=-0.6$ in position 250. The two solitons move against each other, collide and they virtually annihilate themselves leaving in place a decaying breather (a). In (b) we show the dynamic evolution as seen in the ionic sublattice. Since the ionic sublattice has not been initially excited, several oscillatory modes are observed in addition to the traveling ionic deformation.

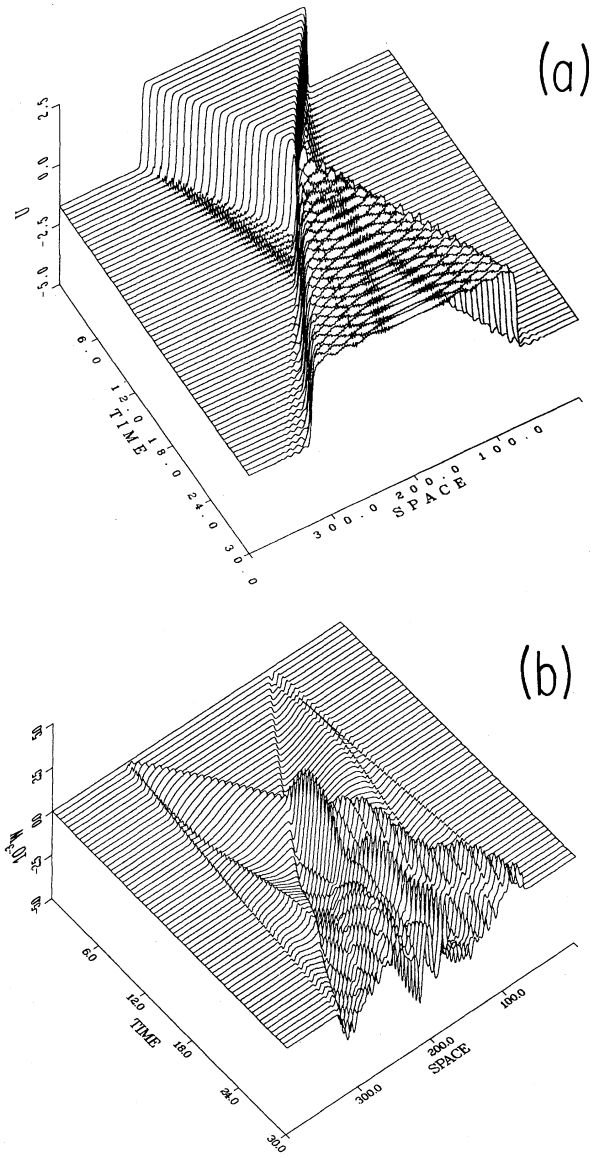

FIG. 8. A small kink-antikink pair with initially large velocities (here both taken equal to 10.0 and in opposite directions) are seen to undergo a collision followed by a reflection (a). In (b) the evolution in the ionic lattice is shown.

move faster than the characteristic velocity v_0, the velocity of sound in the ionic lattice. Because of this, in Fig. 8(b) the second soliton component is not formed and only a small wavelike disturbance follows the kinks. As a result of the collision, large amplitude ionic oscillations are formed that cannot follow the speedy kinks.

Both annihilation and reflection of the small kink-antikink pair can be understood physically in terms of the actual protonic motion in the effective double wells of the hydrogen bonds. Let us assume for simplicity that a kink (antikink) is fairly localized and involves only three adjacent protons. Then, the transition region in a left-right-left state (small kink-antikink pair) involves basically two adjacent hydrogen bonds, both of which have the corresponding protons in the right well of the hydrogen bond. Since the kinks are counterpropagating, the spring connecting these two protons will be compressed. If the velocities before the collision are small, then the collision will affect only these two adjacent protons leading to a decaying oscillation during which the energy released during the collision will be shared by the hydrogen bonds. However, when the initial velocities are much larger, the initial momentum of the adjacent and colliding protons will be transferred to the next neighbors, and, as a result, the latter will move from left to right configurations. This is equivalent to the reflection of the two kinks.

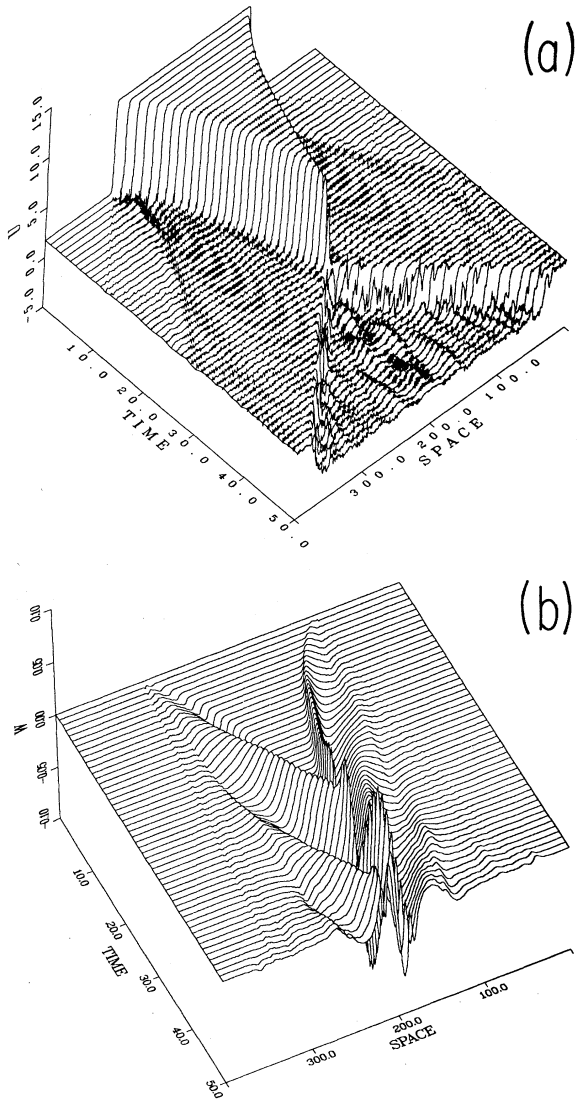

FIG. 9. A pair of large kinks (Bjerrum defects) are placed initially in positions 100 and 300, respectively, with opposite velocities and equal to 10.0 in our dimensionless unit. In (a) we observe that as a result of this collision a small pair of kinks-antikinks is created. In (b) we show the corresponding dynamics in the ionic sublattice.

When a pair of large kinks are counterpropagating in the crystal, the collision properties observed are different. Indeed, for all velocities tested, we observed a conversion of the large pair into a pair of small kink-antikinks. This is in agreement with Ref. 32 as well. The conversion of the large pair into a small one occurs because it is energetically more favorable for the protons to move across a small barrier (the hydrogen bond), rather than across the large barrier (Bjerrum rotations). This behavior is depicted in Fig. 9. We note that the excess of the large kink potential energy is distributed into (a) kinetic energy for the resulting and faster moving small kinks and (b) potential energy in the heavy-ion sublattice that causes large amplitude oscillations. As a result of the inability of heavy ions to follow the speedy kinks, a local oscillatory mode is created.

When a small kink moves against a large kink, we have a collision situation similar to that of a small mass colliding with a large mass. Here, the large kink passes its momentum to the small one, which subsequently reverses its direction of motion.

Finally, when all four kinds of kinks are present in the system, the properties of the system can be understood from the analysis of the individual "elementary" collision. An example of a situation where all four types of defects are present is depicted in Fig. 10.

IV. CONCLUSIONS

We have presented a study of a nonlinear model for the motion of defects in quasi-one-dimensional hydrogen-bonded materials. Although several models have appeared recently addressing the collective dynamics of protons in hydrogen-bonded systems, none of these models can accommodate fully all types of defects that are known experimentally to play an important role in the electrical properties of these systems. The present model introduces in a natural way both types of defects associated with hydrogen-bonded systems. This is accomplished through the introduction of a substrate potential which is doubly periodic. A judicious choice of interaction between the two sublattices constituting the system, leads to an exact solution of the model in the continuum limit, i.e., in the limit when only long-wavelength excitations are present. It was shown that in this limit, two kinds of kink solitons emerge, as a result of the double-sine-Gordon structure of the equation of motion for the protonic sublattice. The smaller kinks of the double-sine-Gordon solution have been associated with a transition (through the small barrier) from one ground state of the system (at $T=0$) to the next one, and correspond to the ionic defects that are present in the hydrogen-bonded materials. The other kind of kink, was shown to lead to rotational or Bjerrum defects in the one-dimensional material.

In the context of the present model, ionic defects of the hydrogen-bonded systems have been associated naturally with the small sine-Gordon-type kinks (type I), and the orientational or Bjerrum defects have been associated with the corresponding large kinks (type II). The following association holds between solitons in the model and defects in the hydrogen-bonded network:

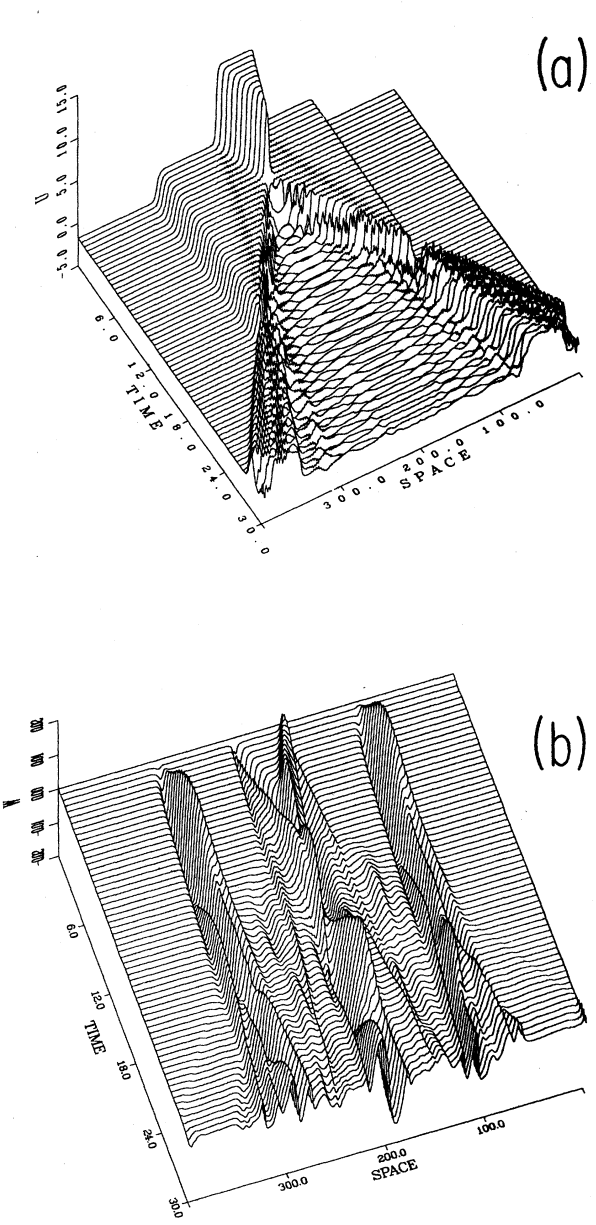

FIG. 10. Representative behavior where all four types of defects are present. For initial velocities we chose the values 0.1, 5.5, −5.5, and −0.1 for small and large kinks, large and small antikinks, respectively. Since the larger pair was given a relatively large initial velocity, its constituent parts collide fast with each other, annihilate, and subsequently create a small soliton pair that moves in the opposite direction. After a few time steps elapse this small pair meets the initially created small pair of solitons and they undergo a collision. In (b) we show the dynamics in the ionic lattice.

kink I$\rightarrow I^-$ ionic defect, kink II$\rightarrow L$ Bjerrum defect ,

antikink I$\rightarrow I^+$ ionic defect, antikink II$\rightarrow D$ Bjerrum defect .

In the case of ice the ions I^-, I^+, are OH^- and H_3O^+, respectively.

When an external electric field is applied in the system, the various defects respond differently, according to their respective charges and effective masses. In particular, the mobilities of small and large solitons are quite different as has been observed in mobility measurements derived through numerical simulations.[26] When an ensemble of defects is present in the system, the individual mobilities as well as the collision properties of the defects will determine the macroscopic conduction properties of the system.

In the present paper we have made a presentation of some of the basic properties of a new physical model pertaining to hydrogen-bonded networks. In particular, in the context of the model we showed that collective dynamics of protons in such a system can be assessed both qualitatively and quantitatively. The double-defect model can be solved analytically (in the continuum limit) in two particular cases, viz., for $\Omega_2=0$ and approximately for $\Omega_2\neq 0$ provided that $v=v_0$. Following these analytical results, we explored numerically the relevant dynamics for meaningful parameter values. Free propagation as well as collision properties of both types of defects have been studied. Analysis of the response of the defects when external electric field is applied in the system as well as dynamics at finite temperatures will be published elsewhere.

The parameter values used in the present paper were chosen as to correspond to the hexagonal crystalline ice form (ice Ih). The coupling constant χ was taken to be quite small[29] in order to avoid dramatic effects in the proton dynamics. Although the exact value of χ for ice is not known with certainty, it is possible that one has to consider substantially larger values, perhaps an order of magnitude larger, than the one chosen for the present study. In this case, an amplification of the role of the ionic substrate is expected.

A serious shortcoming for the present one-dimensional model is the true three-dimensional nature of real solids such as crystalline ice Ih. Although Bernal-Fowler filaments in ice provide quasi-one-dimensional chains, the interaction among these chains must be taken into account in a complete physical model for this system. Nevertheless, the zig-zag, quasi-one-dimensional structure that is exemplified by such filaments in ice, can be found in abundance in nature, especially in biological systems. The electrical properties of such proton dominated networks are similar to those of ice.[33] A particularly good candidate for our model is provided by crystalline hydrogen fluoride.[4] We will report on that system elsewhere.

ACKNOWLEDGMENTS

We would like to thank David W. Brown, Katja Lindenberg, Evita Vulgaris, Peter S. Lomdahl, and David K. Campbell for helpful discussions. G.P.T. would like to thank the Center for Nonlinear Studies at Los Alamos National Laboratory and St.P. the Institute for Nonlinear Science at the University of California at San Diego for their hospitality while this work was in progress. G.P.T. acknowledges the support of National Science Foundation Grant No. DMR 86-19650-A1 and the University of California at San Diego block grant at the San Diego Supercomputer Center.

[1]A. S. Davydov, *Solitons in Molecular Systems* (Reidel, Boston, 1985).
[2]X. Wang, D. W. Brown, K. Lindenberg, and B. J. West, Phys. Rev. A **37**, 3557 (1988).
[3]A. C. Scott, Philos. Trans. R. Soc. London, A Ser. **315**, 423 (1985).
[4]R. W. Jansen, R. Bertoncini, D. A. Pinnick, A. I. Katz, R. C. Hanson, O. F. Sankey, and M. O'Keeffe, Phys. Rev. B **35**, 9830 (1987).
[5]J. F. Nagle, M. Mille, and H. J. Horowitz, J. Chem. Phys. **72**, 3959 (1980).
[6]L. Onsager, Science **156**, 541 (1967); **166**, 1359 (1969).
[7]N. Bjerrum, Science **115**, 385 (1952).
[8]*Physics of Ice,* edited by N. Riehl, B. Bullemer, and H. Engelhart (Plenum, New York, 1969).
[9]*Physics and Chemistry of Ice,* edited by F. Whalley, S. J. Jones, and L. W. Gold (Royal Society of Canada, Ottawa, 1973).
[10]P. B. Hobs, *Ice Physics* (Clarendon, Oxford, 1974).
[11]L. Glasser, Chem. Rev. **75**, 21 (1975).
[12]J. H. Weiner and A. Askar, Nature **226**, 842 (1970).
[13]V. Ya. Antonchenko, A. S. Davydov, and A. V. Zoloaryuk, Phys. Status Solidi B **115**, 631 (1983).
[14]J. D Bernal and R. H. Fowler, J. Chem. Phys. **1**, 515 (1933).
[15]E. W. Laedke, K. H. Spatschek, M. W. Wilkens, Jr., and A. V. Zolotaryuk, Phys. Rev. A **32**, 1161 (1985).
[16]H. Weberpals and K. H. Spatscheck, Phys. Rev. A **36**, 2946 (1987).
[17]M. Peyrard, St. Pnevmatikos, and N. Flytzanis, Phys. Rev. A **36**, 903 (1987).
[18]A. V. Zolotaryuk, K. H. Spatschek, and E. W. Laedke, Phys. Lett. A **101**, 517 (1984).
[19]St. Pnevmatikos, Phys. Lett. A **122**, 249 (1987).
[20]J. Halding and P. S. Lomdahl. Phys. Rev. A **37**, 2608 (1988).
[21]G. P. Tsironis, E. Nylund, and K. Lindenberg (unpublished).
[22]O. E. Yanovitki and E. S. Kryacho (unpublished).
[23]R. J. Bagley, St. Pnevmatikos and D. K. Campbell (unpublished).
[24]L. N. Kristoforov, A. V. Zolotaryuk, Phys. Status Soildi B

146, 487 (1988).
[25]St. Pnevmatikos, Phys. Rev. Lett. **60**, 1534 (1988).
[26]G. P. Tsironis and St. Pnevmatikos (unpublished).
[27]S. Yomosa, J. Phys. Soc. Jpn. **52**, 1866 (1983); **51**, 3318 (1982); Y. Kasimori, F. Chien, and K. Nishimoto, Chem. Phys. **107**, 389 (1986); Y. Kashimori, T. Kikuchi, and K. Nishimoto, J. Chem. Phys. **77**, 1904 (1982); St. Pnevmatikos, N. Flytzanis, and R. Bishop, J. Phys. C **20**, 2829 (1987).
[28]M. A. Collins, A. Blumen, J. F. Currie, and J. Ross, Phys. Rev. B **19**, 3630 (1979).
[29]In the simulations we used the values 85.00 and 0.032 for χ_1 and χ_2, respectively.
[30]K. M. DeLeonardis and S. E. Trullinger, Phys. Rev. B **27**, 1867 (1983).
[31]C. A. Condat, R. A. Guyer, and M. D. Miller, Phys. Rev. B **27**, 474 (1983).
[32]D. K. Campbell, M. Peyrard, and P. Sodano, Physica D **19**, 165 (1986).
[33]V. H. Schmidt, J. E. Drumheller, and F. L. Howell, Phys. Rev. B **4**, 4582 (1971); J. Vanderkooy, J. D. Cuthbert, and H. E. Petch, Can. J. Phys. **42** 1871 (1964); J. Bacon and D. P. Santry, J. Chem. Phys. **56**, 2011 (1972); A. Kawada, A. R. McGhie, and M. M. Labes, J. Chem. Phys. **52**, 3121 (1970); R. Blinc, V. Dimic, J. Petrovsek, and E. Pirkmajer, Phys. Lett. A **26**, 8 (1967); D. Oesterhelt and W. Stoeckenious, Proc. Nat. Acad. Sci. USA **70**, 2853 (1973).